Fast approximate calculation of multiply scattered lidar returns

Robin J. Hogan

An efficient method is described for the approximate calculation of the intensity of multiply scattered lidar returns. It divides the outgoing photons into three populations, representing those that have experienced zero, one, and more than one forward-scattering event. Each population is parameterized at each range gate by its total energy, its spatial variance, the variance of photon direction, and the covariance of photon direction and position. The result is that for an N-point profile the calculation is $O(N^2)$ efficient and implicitly includes up to N-order scattering, making it ideal for use in iterative retrieval algorithms for which speed is crucial. In contrast, models that explicitly consider each scattering order separately are at best $O(N^m/m!)$ efficient for m-order scattering and often cannot be performed to more than the third or fourth order in retrieval algorithms. For typical cloud profiles and a wide range of lidar fields of view, the new algorithm is as accurate as an explicit calculation truncated at the fifth or sixth order but faster by several orders of magnitude. © 2006 Optical Society of America

OCIS codes: 290.0290, 290.4210, 280.3640, 290.1090.

1. Introduction

Lidar is a powerful tool for deriving the properties of clouds and aerosols, but the main difficulty to overcome is the significant extinction of the lidar beam in its path through the medium, and in most situations one must take into account multiple scattering. The inversion of the lidar signal is assisted when performed in synergy with other instruments, and promising methods have been developed using a radiometer[1,2] and cloud radar.[3–5] For a rigorous treatment of errors when combining measurements from different sources, a variational approach[6] should be used, which involves an initial guess of the profile of atmospheric properties being iteratively refined based on its ability to synthesize the measurements. A key ingredient is a fast lidar forward model, which in addition to predicting the attenuated backscatter profile from a profile of extinction and particle size, must provide the Jacobian, i.e., the derivative of the predicted backscatter at each height with respect to each of the input variables at all other heights. The new spaceborne lidar[7] and radar[8] will record profiles continuously every 0.1 s, so for the data to be processed in a satisfactory time, an accurate lidar forward model is required that runs in less than 0.001 s.

In this paper such a method is described. Key to the speed of the algorithm are the following assumptions, which were also made by Eloranta[9] in the formulation of his algorithm: (i) Both the laser divergence and the forward scattering diffraction peak may be represented as Gaussians, and (ii) the scatterers are much larger than the wavelength, such that the forward-scattered lobe is narrow and the received power is dominated by photons that may have undergone many small-angle forward scatterings on both the outgoing and return journeys, but only one large-angle backscattering event. The latter is sometimes referred to as the quasi-small-angle approximation.[10] The following assumptions are common with Eloranta, although in principle they could be relaxed in a future version: (iii) The phase function is isotropic in the backscatter direction, (iv) the extra path length of multiply scattered photons may be neglected, and (v) the lidar is monostatic so that the problem has azimuthal symmetry. To achieve $O(N^2)$ efficiency for an N-point profile, it is necessary to divide the outgoing photon distribution into three populations: unscattered, singly forward-scattered, and multiply forward-scattered photons (a similar division was also employed by Bissonnette,[11] although his subsequent derivation was quite different). The backscatter from the first two populations is calculated explicitly, but the backscatter from the third is calculated more approximately by parame-

R. J. Hogan (r.j.hogan@reading.ac.uk) is with the Department of Meteorology, University of Reading, Reading RG6 6BB, UK.

Received 18 November 2005; revised 5 March 2006; accepted 12 March 2006; posted 13 March 2006 (Doc. ID 66127).

0003-6935/06/235984-09$15.00/0

terizing each population by four variables at each gate and sequentially considering how forward scattering at each gate modifies the variables at subsequent gates. This approximation is justified *a posteriori* by the good agreement found with the much more computationally expensive Eloranta model run to a high order of scattering.

In Section 2 the geometry of the problem is introduced, and in Section 3 the explicit single- and double-scattering calculation is described. Section 4 then describes the novel approach to calculating triple and higher-order scattering. In Section 5 the accuracy of the algorithm is compared with Eloranta's model, and in Section 6 benchmark computations are carried out to assess its speed.

2. Background

The formulation of the algorithm is greatly simplified by the use of the equivalent-medium theorem, which has been proved to be valid under the quasi-small-angle approximation.[10,12] This theorem states that the backscatter measured in a medium is the same as that from an equivalent hypothetical medium that has twice the extinction and scattering coefficients (but the same phase function) as the true medium on the outward journey but zero extinction and scattering on the return journey. Thus the two-way problem is transformed into a simpler one-way propagation problem. It should be stressed that the computational speed of the algorithm is achieved primarily by the parameterizations described in Section 4, not by the use of this theorem; indeed, an earlier version of this algorithm was formulated without the use of this theorem and was only marginally slower.

Suppose a lidar emits a short pulse of total energy P_0 in a Gaussian beam with a $1/e$ angular half-width of ρ_l, then at a distance R from the instrument, the energy density of unscattered photons (in J m^{-2}) in the equivalent medium is a function of distance perpendicular to the laser axis, s,

$$E_u(R, s) = \frac{P_0 \exp[-2\delta(R)]}{\pi\rho_l{}^2R^2} \exp\left(-\frac{s^2}{\rho_l{}^2R^2}\right), \tag{1}$$

where $\delta(R)$ is the optical depth of the true atmosphere between the laser and range R, and the prefix of a factor of 2 is due to the use of the equivalent medium. If there are additional forward-scattering events in this range then they will also contribute to the outgoing photon distribution at R. Following Eloranta[9] a cloud or aerosol layer of thickness dr a distance r from the laser (where $r < R$) is considered. If it has a true extinction coefficient $\alpha(r)$, then the value in the equivalent medium will be $2\alpha(r)$, but this factor of 2 is then removed by the fact that, according to diffraction theory, half of the extinguished energy will be scattered into a narrow forward lobe. This lobe may be approximated by a Gaussian, the angular width of which is characterized by $\Theta(r)$, defined as the $1/e$ angular half-width of the scattered energy or equivalently the root-mean-squared forward-scattering angle. The additional spatial variance at range R is given by $\Theta^2(R - r)^2$, so by convolving the two Gaussians the forward-scattering contribution of layer dr to the energy density at R is obtained:

$$\mathrm{d}E_s(R, s) = \frac{P_0 \exp[-2\delta(R)]}{\pi\rho_l{}^2R^2 + \pi\Theta^2(R-r)^2} \times \exp\left[-\frac{s^2}{\rho_l{}^2R^2 + \Theta^2(R-r)^2}\right]\alpha(r)\mathrm{d}r, \tag{2}$$

where the subscript in dE_s denotes singly forward-scattered photons. Note that the phase function for Rayleigh-scattering air molecules is much more isotropic than clouds or aerosols, so it is safe to assume that molecular scattering does not contribute significantly to the forward-scattered lobe. Hence α in Eq. (2) should be the true extinction coefficient of the cloud and aerosol particles only. It should be stressed that no assumption has been made regarding whether the particles are absorbing; half the extinguished energy is diffracted into the forward lobe, but the algorithm does not care if the remaining half is absorbed or scattered, except for the small fraction that is scattered back to the receiver.

To obtain the distribution at R of all photons that have undergone a single forward-scattering event somewhere previously in the profile, Eq. (2) would need to be integrated over range r. To include the photons that have undergone two forward-scattering events, the problem then becomes a 2D integration since for each layer dr_i that the photon is scattered from a first time, one must consider all possible layers dr_j that it may be scattered from a second time. Likewise, the explicit calculation of m forward-scattering events by this method is an m-dimensional integration. This is the essence of the Eloranta[9] formulation, which is O($N^m/m!$) efficient for m-order scattering (now including the single backscatter event and the additional loop to calculate the apparent backscatter at each of the N points). It was assumed by Eloranta, and is also assumed here, that the backscatter is dominated by photons that have undergone one backscattering event but may have been scattered forward many times [assumption (ii) in Section 1]. Figure 1 shows the trajectory of a single photon emitted by the lidar and scattered at a range r_i.

It is now shown how Θ_i^2 is obtained. For a single sphere of radius a in the quasi-small-angle approximation, the Fraunhofer diffraction theory[13] provides the amplitude $F(\theta)$ of the forward-scattered wave as a function of scattering angle θ, the square of which is the phase function $\mathcal{P}(\theta)$ normalized by its peak value $\mathcal{P}(0)$:

$$\frac{\mathcal{P}(\theta)}{\mathcal{P}(0)} = [F(\theta)]^2 = \left[\frac{2J_1(2\pi\theta a/\lambda)}{2\pi\theta a/\lambda}\right]^2, \tag{3}$$

where J_1 is the Bessel function of the first kind, and λ is the wavelength of the radiation. This may be ap-

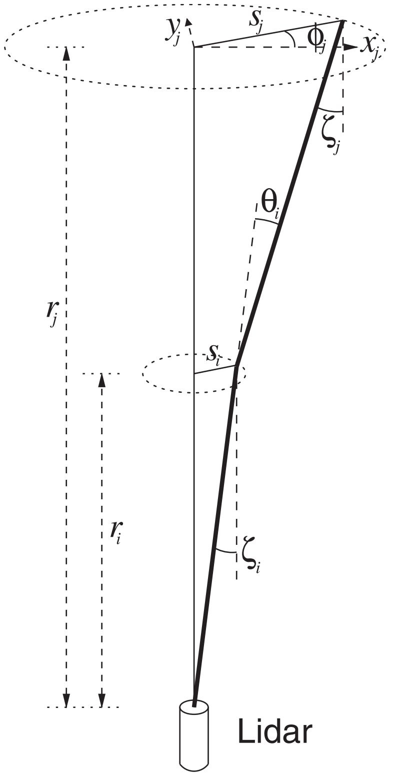

Fig. 1. Schematic showing the trajectory of a photon emitted by the laser such that when it arrives at range r_i it has a lateral displacement s_i and an angle ζ_i relative to the lidar axis. It is then scattered by an angle θ_i such that on reaching range r_j it has lateral displacement s_j and angle ζ_j. In Cartesian coordinates the displacement is written as (x_j, y_j).

proximated by a Gaussian $\mathcal{P}(\theta)/\mathcal{P}(0) \simeq \exp(-\theta^2/\Theta^2)$, where the variance of the scattering angle is given by $\Theta^2 = \lambda^2/(\pi^2 a^2)$, or equivalently $\Theta^2 = \lambda^2/(\pi G)$, where G is the particle cross-sectional area. The Gaussian expression has the same peak magnitude and the same total energy as Eq. (3) and accurately represents the main Fraunhofer lobe as demonstrated by the fact that a Taylor expansion of Eq. (3) at approximately $\theta = 0$ shares the same first three terms as an expansion of the Gaussian expression. For nonspherical particles the definition of Θ^2 in terms of G is used.

For a distribution of particles, the variance Θ^2 arising from each particle is weighted by its contribution to the energy in the forward lobe, which is proportional to the extinction cross section σ_e. Hence the variance for the whole distribution is given by

$$\Theta^2 = \frac{\lambda^2}{\pi}\int_0^\infty n(G)\frac{\sigma_e(G)}{G}\mathrm{d}G \bigg/ \int_0^\infty n(G)\sigma_e(G)\mathrm{d}G, \quad (4)$$

where $n(G)\mathrm{d}G$ is the number concentration of particles with cross-sectional areas between G and $G + \mathrm{d}G$. In the geometric optics approximation, $\sigma_e \simeq 2G$, so this simplifies to

$$\Theta^2 = \frac{\lambda^2}{\pi\langle G\rangle}, \qquad \text{or} \qquad \Theta = \frac{\lambda}{\pi a_G}, \quad (5)$$

where $\langle G\rangle$ is the mean cross-sectional area of the particles in the distribution and a_G is the equivalent-area radius of the size distribution such that $\pi a_G{}^2 = \langle G\rangle$. It should be noted that the distribution of scattering angles resulting from a broad size distribution is not strictly Gaussian because it consists of the sum of many distributions of different widths. In approximating it as a Gaussian with a width Θ defined above, I have chosen to preserve the energy and variance of the true distribution but will necessarily have underestimated the peak value of the phase function. In his derivation of the appropriate mean particle size to use, Eloranta[9] chose instead to preserve the energy and the peak value, which results in the variance being somewhat underestimated.

Now the detection of returned photons is considered. Suppose at range R we have managed to obtain the total distribution of outgoing photons $E(R, s)$ (scattered and unscattered). In the equivalent medium, the return journey of any backscattered photons is in vacuum, so the only photons that can be detected by a telescope with a half-angle field of view of ρ_t are those photons with a lateral distance of $s < \rho_t R$. Assuming the phase function to be isotropic near 180°, the energy $\mathrm{d}Q$ received by the telescope due to backscattering from a layer of thickness $\mathrm{d}R$ with backscatter coefficient β (both from particles and air molecules) is found by integration over s and the angle round the cone ϕ:

$$\mathrm{d}Q(R) = \frac{A_t\beta(R)\mathrm{d}R}{R^2}\int_0^{2\pi}\int_0^{\rho_t R} E(R,\ s)s\mathrm{d}s\mathrm{d}\phi = \frac{2\pi A_t\beta(R)\mathrm{d}R}{R^2}\int_0^{\rho_t R} E(R,\ s)s\mathrm{d}s, \quad (6)$$

where A_t is the area of the telescope aperture. So that the calculation is $\mathrm{O}(N^2)$ efficient, it is necessary to divide E into the sum of three photon populations, unscattered E_u, singly forward-scattered E_s, and multiply forward-scattered E_m. The corresponding energies received from a thin layer are denoted $\mathrm{d}Q_u$, $\mathrm{d}Q_s$, and $\mathrm{d}Q_m$.

3. Treatment of Single and Double Scattering

For single scattering the lidar equation is simply used to obtain the apparent backscatter due to single scattering, $\hat{\beta}_1$, as a function of the unattenuated backscatter coefficient β:

$$\hat{\beta}_1(R) = \beta(R)\exp[-2\delta(R)]. \quad (7)$$

Care should be taken in discretizing this relationship: If gate i represents ranges from R to $R + \Delta R$, and both backscatter coefficient (β_i) and extinction coefficient (α_i) are constant within the gate such that

$\delta(R + \Delta R) = \delta(R) + \alpha_i \Delta R$, then the apparent backscatter integrated across the gate is

$$\hat{\beta}_{1,i} = \frac{1}{\Delta R}\int_R^{R+\Delta R} \beta(R')\exp[-2\delta(R')]\mathrm{d}R' \tag{8}$$

$$= \beta_i \exp[-2\delta(R)]\,\frac{1-\exp(-2\alpha_i\Delta R)}{2\alpha_i\Delta R}. \tag{9}$$

For the apparent backscatter due to double scattering (i.e., one forward-scattering event and one backscatter event), $\hat{\beta}_2$, it is convenient to normalize by $\hat{\beta}_1$ such that the terms before the integral in Eq. (6) are eliminated:

$$\frac{\hat{\beta}_2(R)}{\hat{\beta}_1(R)} = \frac{\mathrm{d}Q_s}{\mathrm{d}Q_u} = \int_0^{\rho_t R} E_s(R,\ s)s\mathrm{d}s \Bigg/ \int_0^{\rho_t R} E_u(R,\ s)s\mathrm{d}s, \tag{10}$$

where $\mathrm{d}Q_s$ and $\mathrm{d}Q_u$ are the received energies from a thin layer due to photons that have been singly forward scattered and not forward scattered, respectively. Noting that $E_s(R, s) = \int_0^R [\mathrm{d}E_s(R, s)/\mathrm{d}r]\mathrm{d}r$, one can use Eqs. (1) and (2) to obtain

$$\hat{\beta}_2(R)/\hat{\beta}_1(R) = \left[1-\exp(-\rho_t^{\,2}/\rho_l^{\,2})\right]^{-1}\int_0^R \left\{1-\exp\left[-\frac{\rho_t^{\,2}R^2}{\rho_l^{\,2}R^2+\Theta_i^{\,2}(R-r)^2}\right]\right\}\alpha(r)\mathrm{d}r. \tag{11}$$

This is the same as the double-scattering formulation of Eloranta,[9] and for N range gates the speed of the calculation is proportional to N^2.

4. Treatment of Triple- and Higher-Order Scattering

To calculate the apparent backscatter due to triple- and higher-order scattering, the distribution E_m of outgoing photons that have been forward scattered more than once needs to be estimated. This is achieved efficiently by parameterizing it as a Gaussian at each range gate. To calculate the parameters of the Gaussian, one needs to consider forward scattering from each previous gate, considering both E_m at that gate and the singly forward-scattered distribution E_s. The distribution E_s is in turn parameterized as a Gaussian and fed by forward scattering from the unscattered distribution E_u at earlier gates. This process is illustrated schematically in Fig. 2.

Thus a handful of parameters are required to represent these three distributions at each range gate. The algorithm proceeds by considering each range gate in turn (the outer loop). The variables at gate i are first used to modify the variables at all subsequent gates j (the inner loop) to represent the outgoing photons that are forward scattered at i and reach j without any further forward-scattering events. Then the variables at i (which have already been modified by forward scattering from all previous gates) are used to estimate the measured backscatter at this gate due to triple- and higher-order scattering, $\hat{\beta}_{3+}$. This procedure is then repeated at gate $i + 1$. Hence it can be seen that the calculation is $O(N^2)$ efficient despite the fact that scattering to a much higher order than second is accommodated. However, inaccuracies arise due to inexact representation of the photon distribution at each range gate.

The shape of each of the three populations is characterized by two variables: its total energy and its variance. The total energy of population k (which may be u, s, or m), P_k, is given by

$$P_k(R) = 2\pi\int_0^\infty E_k(R,\ s)s\mathrm{d}s. \tag{12}$$

However, it is simpler to consider the total energy relative to the energy in the unscattered beam, which gives us our first variable $\hat{P}_k = P_k/P_u$. This avoids the need to evaluate the $\exp[-2\delta(R)]$ term repeatedly. It also means that $\hat{P}_u$ is unity at all heights. The width of the distribution is characterized by its second moment, i.e., the mean-squared lateral distance of the photons from the lidar axis:

$$\overline{s^2}_k(R) = \frac{2\pi}{P_k(R)}\int_0^\infty s^2E_k(R,\ s)s\mathrm{d}s. \tag{13}$$

Two additional variables are required for each population to accurately predict the effect of forward scattering at one range on the distribution of photons at another. The first of these is the second moment of the distribution of photon direction angles relative to the lidar axis, $\overline{\zeta^2}$. The second is the covariance of the photon direction with its position relative to the lidar axis, $\overline{s\zeta}$. Figure 1 illustrates the meaning of s and ζ for a single photon.

All photon populations originate ultimately from the unscattered population E_u. In the quasi-small-angle approximation, the four coefficients defining E_u are

$$\begin{aligned}\hat{P}_u &= 1, & \overline{s^2}_u &= r^2\rho_l^{\,2},\\ \overline{\zeta^2}_u &= \rho_l^{\,2}, & \overline{s\zeta}_u &= r\rho_l^{\,2}.\end{aligned} \tag{14}$$

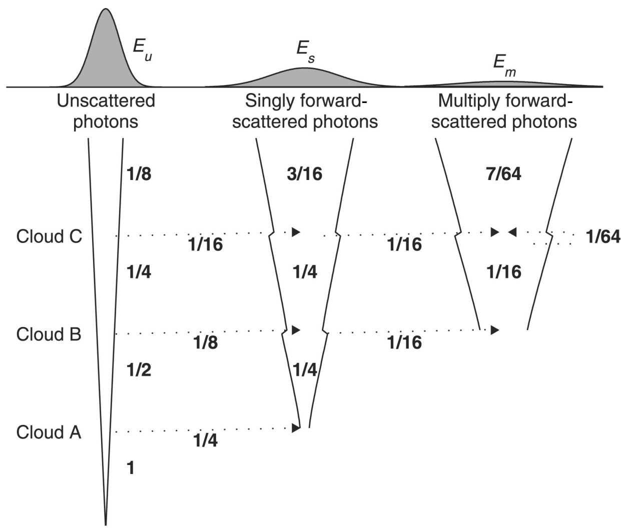

Fig. 2. Schematic illustrating the representation of the outgoing photon distribution E as the sum of three populations. In this example there are three infinitesimally thin clouds A–C, each with an optical depth (in the equivalent medium) of 0.69 such that, of the incoming radiation, half is unscattered, one fourth is forward scattered and is transferred to the next population (indicated by the dotted lines), and the remaining one fourth is scattered in other directions and lost to the system (except for the very small fraction that is backscattered to the detector). The numbers in bold indicate the fractions of the initial energy (i.e., P/P_0) that remain at each stage. The thin solid lines depict the standard deviations of each population, with the notches in the E_s and E_m cones indicating where the standard deviation has been reduced by the addition of photons from one of the other populations. The three distributions in gray at the top show the representation of each outgoing population by a Gaussian with the correct mean and standard deviation.

Note that the covariance term is derived by recognizing that for the unscattered distribution, the photon angle is perfectly correlated with the photon position, i.e., correlation coefficient $\overline{s\zeta}/(\overline{s^2}\ \overline{\zeta^2})^{1/2} = 1$.

Next how forward scattering at range gate i (of length Δr) affects all subsequent range gates j is considered. Forward scattering of the population E_i (which might be E_u, E_s, or E_m) at i leads to an increment to population E_j (which might be E_s or E_m) at j, which is denoted as ΔE_j. Note that forward-scattered photons from population E_m at gate i remain in E_m at gate j (illustrated by the arrow labeled 1/64 in Fig. 2), but the variables describing this population are modified approximately. The four variables describing the incremental distribution are given by

$$\Delta\hat{P}_j = \hat{P}_i\alpha_i\Delta r, \tag{15}$$

$$\Delta\overline{s^2}_j = \overline{s^2}_i + \left(\overline{\zeta^2}_i + \Theta_i^2\right)(r_j - r_i)^2 + 2\overline{s\zeta}_i(r_j - r_i), \tag{16}$$

$$\Delta\overline{\zeta^2}_j = \overline{\zeta^2}_i + \Theta_i^2, \tag{17}$$

$$\Delta\overline{s\zeta}_j = \overline{s\zeta}_i + \left(\overline{\zeta^2}_i + \Theta_i^2\right)(r_j - r_i). \tag{18}$$

Equation (15) arises because half of the extinguished radiation is in the forward lobe, but the factor of 1/2 disappears because an equivalent medium with an extinction coefficient of $2\alpha_i$ is being considered. Equation (16) may be derived by considering the geometry depicted in Fig. 1. Suppose a single photon at gate i has position (x_i, y_i) and direction $(\zeta_{x,i}, \zeta_{y,i})$ relative to the lidar axis. If it is scattered by a small angle $(\theta_{x,i}, \theta_{y,i})$ then its position at gate j is given by

$$x_j = x_i + (\zeta_{x,i} + \theta_{x,i})(r_j - r_i) \tag{19}$$

and similarly for y_j. Taking the square of both sides and averaging over all photons scattered at i yields

$$\overline{x_j^2} = \overline{x_i^2} + \left(\overline{\zeta_{x,i}^2} + \overline{\theta_{x,i}^2}\right)(r_j - r_i)^2 + 2\overline{x_i\zeta_{x,i}}(r_j - r_i), \tag{20}$$

recognizing that, as the scattering angle is uncorrelated with the original position and direction of the photon, the covariance terms $\overline{\zeta_{x,i}\theta_{x,i}}$ and $\overline{x_i\theta_{x,i}}$ are both zero. From the definitions $\overline{s^2} = \overline{x^2} + \overline{y^2}$, $\overline{\zeta^2} = \overline{\zeta_x^2} + \overline{\zeta_y^2}$, $\overline{s\zeta} = \overline{x\zeta_x} + \overline{y\zeta_y}$, and $\Theta^2 = \overline{\theta_x^2} + \overline{\theta_y^2}$, Eq. (16) is obtained. A similar procedure may be used to derive Eqs. (17) and (18).

For the singly forward-scattered distribution, the definitions in Eq. (14) enable us to simplify Eqs. (15)–(18) to

$$\Delta\hat{P}_{s,j} = \alpha_i\Delta r, \tag{21}$$

$$\Delta\overline{s^2}_{s,j} = \rho_l^2 r_j^2 + \Theta_i^2(r_j - r_i)^2, \tag{22}$$

$$\Delta\overline{\zeta^2}_{s,j} = \rho_l^2 + \Theta_i^2, \tag{23}$$

$$\Delta\overline{s\zeta}_{s,j} = \rho_l^2 r_j + \Theta_i^2(r_j - r_i). \tag{24}$$

The incremental distributions are then added to the appropriate existing population at gate j. The total energy is simply incremented by $\Delta\hat{P}$:

$$\hat{P}_j \leftarrow \hat{P}_j + \Delta\hat{P}_j. \tag{25}$$

The other three variables are weighted summations, but in practice it is more efficient to hold the products $\hat{P}_j\overline{s^2}_j$, $\hat{P}_j\overline{\zeta^2}_j$, and $\hat{P}_j\overline{s\zeta}_j$ in memory such that the weighted summations become

$$\left(\hat{P}_j\overline{s^2}_j\right) \leftarrow \left(\hat{P}_j\overline{s^2}_j\right) + \Delta\hat{P}_j \times \Delta\overline{s^2}_j, \tag{26}$$

and similarly for $\hat{P}_j\overline{\zeta^2}_j$ and $\hat{P}_j\overline{s\zeta}_j$.

In this way, the three populations E_u, E_s, and E_m may be built up one gate at a time. Each is defined by four variables, but from Eq. (14) it can be seen that the variables defining E_u are predefined from the lidar instrument parameters. Hence the eight variables to keep track of at each gate are $\hat{P}_s$, $\hat{P}_m$, $(\hat{P}_s\overline{s^2}_s)$, $(\hat{P}_m\overline{s^2}_m)$, $(\hat{P}_s\overline{\zeta^2}_s)$, $(\hat{P}_m\overline{\zeta^2}_m)$, $(\hat{P}_s\overline{s\zeta}_s)$, and $(\hat{P}_m\overline{s\zeta}_m)$. An important point to note is that, subject to assumptions (i), (ii), and (iv) in Section 1 (common with Eloranta[9]), these variables are calculated exactly. It is only in the final step, in which E_m is characterized by a Gaussian,

$$E_m(R,\ s) = \frac{P_m}{\pi \overline{s^2}_m} \exp\left(-\frac{s^2}{\overline{s^2}_m}\right), \tag{27}$$

that an additional approximation is made. Note that Eq. (27) satisfies the constraints given by Eqs. (12) and (13). The apparent backscatter due to triple- and higher-order scattering, normalized by $\hat{\beta}_1$, is then found in the same way as for double scattering in Section 3:

$$\frac{\hat{\beta}_{3+}(R)}{\hat{\beta}_1(R)} = \frac{\mathrm{d}Q_m}{\mathrm{d}Q_u} = \hat{P}_m \frac{1 - \exp\left(-\rho_t^2 R^2/\overline{s^2}_m\right)}{1 - \exp(-\rho_t^2/\rho_l^2)}. \tag{28}$$

The full apparent backscatter $\hat{\beta}(R)$ may then be calculated by summing the three components given by Eqs. (7), (10), and (28). Note that we could have also approximated E_s as a Gaussian and taken the same approach to derive $\hat{\beta}_2(R)/\hat{\beta}_1(R)$ from $\hat{P}_s$ and $\overline{s^2}_s$. However, this would be no more efficient than using Eq. (10) but would be less accurate because Eq. (10) implicitly treats E_s as the sum of Gaussians of different widths, rather than just one Gaussian.

As will be seen in Section 5, Eq. (28) performs well provided that the quasi-small-angle assumption is valid. In the case of aerosol particles viewed with a visible-wavelength lidar, the particle size and the wavelength are of the same order and this assumption is violated. When separate layers of aerosols and cloud particles are present in the same profile, the greatly differing forward-scattering lobe widths result in highly non-Gaussian photon distributions; the photons scattered widely by the aerosols are far less likely to return to the telescope than those scattered into a narrow forward lobe by the cloud particles. Applying the single Gaussian approximation then smears out the peak due to the cloud particles, and the degree of multiple scattering is underestimated. This problem may be solved in a crude but effective manner by setting the energy in the incremental forward-scattered distributions emanating from aerosol-filled gates to zero, i.e., $\Delta\hat{P}_s = \Delta\hat{P}_m = 0$ in Eq. (15). Note that a forward-scattered distribution still remains at subsequent gates; it is simply not incremented by the aerosol layers. An effective criterion to trigger this action is $\Theta > 0.1$ rad. The aerosols are then being treated in the same way as molecules but with one important difference, namely, that their contribution to double scattering is still represented accurately by Eq. (11). Because the multiple scattering in aerosol layers is dominated by double scattering, this is found to be a satisfactory assumption.

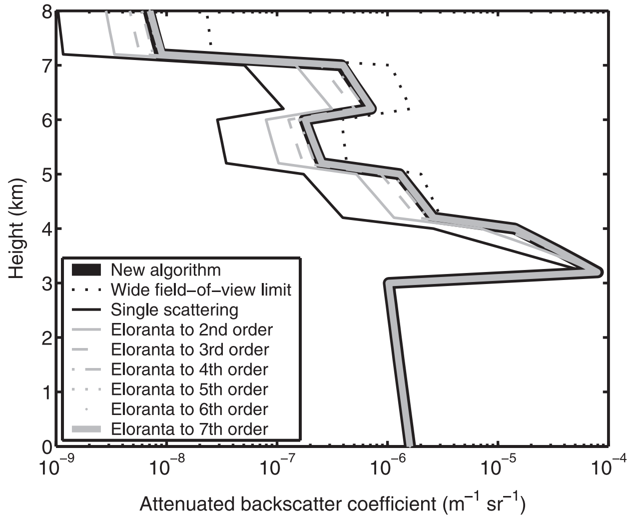

Fig. 3. Comparison of the new algorithm and the Eloranta (Ref. 9) formulation for ground-based 532 nm lidar observing an ice cloud with extinction coefficients of 2, 0.5, 0.1, and 0.5 km^{-1} in the height ranges 4–5, 5–6, 6–7, and 7–8 km, respectively. The black lines show the apparent backscatter estimated by the new algorithm, $\hat{\beta}$ (thick line), together with the theoretical extremes of single scattering only (thin solid line), and all the forward-scattered photons remaining in the telescope field of view (dotted line). The gray lines show the predictions by the Eloranta model including successively higher orders of scattering.

5. Comparison with Eloranta's Model

The new algorithm has been compared to Eloranta's model for a wide range of cloud profiles and lidar parameters. In this section I present two profiles to illustrate the strengths and weaknesses of the new algorithm. Comparisons of Eloranta's model with Monte Carlo calculations have already been carried out[5,9] and verify its applicability, so there is no need to perform such runs here.

First considered is a 4 km thick ice cloud with an optical depth of 3.1, a constant equivalent-area radius (a_G) of 100 μm and a constant extinction-to-backscatter ratio of 20 sr. It is observed by a ground-based 532 nm lidar with a half-angle laser divergence of $\rho_l = 0.5$ mrad and a half-angle telescope field of view of $\rho_t = 0.75$ mrad. Molecular scattering is considered to follow an inverse exponential profile with a scale height of 8 km and a surface backscatter coefficient of $1.6 \times 10^{-6}\ \mathrm{m}^{-1}\ \mathrm{sr}^{-1}$, appropriate for a pressure of 1013 hPa and a temperature of 15 °C. Figure 3 shows a comparison between the new algorithm and Eloranta's model truncated at a number of different scattering orders, with both algorithms calculated at a resolution of 200 m. It can be seen that the new algorithm reproduces the high-order Eloranta calculation to within 4%, which only converges when taken to fifth- or sixth-order scattering. The computational times of such calculations are provided in Section 6.

The thin black lines in Fig. 3 represent the two extremes between which a multiple scattering solution must lie; the solid line shows the single-

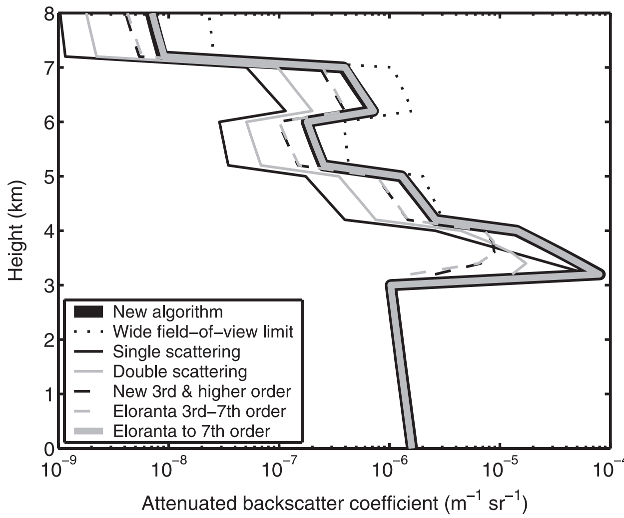

Fig. 4. As in Fig. 3, but showing the three separate contributions toward the apparent backscatter in the new algorithm: The single- and double-scattering components, $\hat{\beta}_1$ and $\hat{\beta}_2$, are common between the new algorithm and that of Eloranta so only one line is shown for each. The prediction of third- and higher-order scattering by the new algorithm, $\hat{\beta}_{3+}$ (black dashed line), is compared with the same prediction by Eloranta's model for scattering up to the seventh order (gray dashed line).

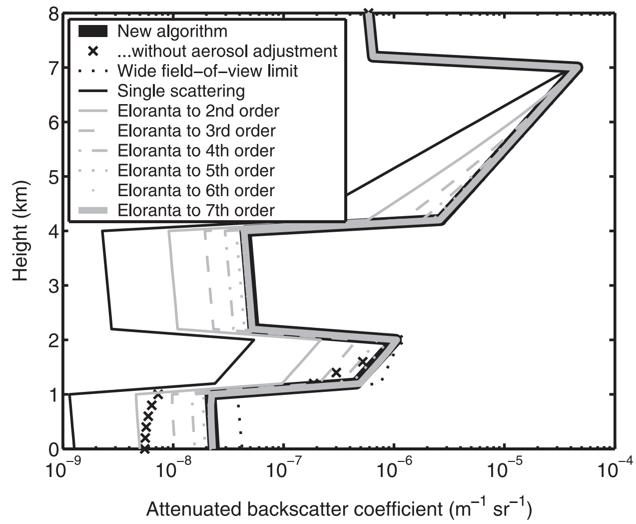

Fig. 5. As in Fig. 3, but for the spaceborne 532 mm CALIPSO lidar at an altitude of 700 km. The ice cloud between 4 and 7 km has a constant extinction coefficient of 1 km^{-1} and a_G of 100 μm. It overlies a 1 km thick aerosol layer with an extinction coefficient of 0.5 km^{-1} and a_G of 0.5 μm. The crosses show the apparent backscatter when forward scattering from the aerosol layer is included in the calculation of $\hat{\beta}_{3+}$, i.e., without the aerosol adjustment described at the end of Section 5.

scattering case [Eq. (7)], appropriate for a lidar with a field of view small enough that all forward-scattered photons escape and are not returned to the telescope. The dotted line shows the wide field-of-view limit, where all forward-scattered photons remain in the telescope field of view. In this case, the apparent backscatter may be calculated easily by using Eq. (7) but halving the optical depth that is due to clouds or aerosols.

As discussed previously, the new algorithm splits the apparent backscatter into the contributions from single scattering ($\hat{\beta}_1$), double scattering ($\hat{\beta}_2$), and scattering orders of 3 and higher ($\hat{\beta}_{3+}$). The first two components are calculated in exactly the same way as the Eloranta formulation (Section 3), whereas the third is calculated in a more approximate fashion that enables it to retain $O(N^2)$ efficiency (Section 4). The dashed lines in Fig. 4 compare $\hat{\beta}_{3+}$ calculated by the new algorithm with that calculated from summing the separate scattering orders from 3 to 7 calculated explicitly by the Eloranta algorithm. The difference in the first cloudy gate is believed to be due to the slightly different ways the equations are discretized and results in a less than 2% difference in the total apparent backscatter $\hat{\beta}$. The slight deviation at the top of the profile results in only a 4% difference in $\hat{\beta}$.

Calculations have been performed using the same cloud profile but with the laser divergence and telescope field of view varied between 0.005 and 50 mrad, and the agreement between the new algorithm and high-order Eloranta calculations is equally good. This would seem to justify the approximation made in Section 4 that the singly and multiply forward-scattered distributions, E_s and E_m, may be described by Gaussians.

To illustrate the performance of the algorithm when the quasi-small-angle approximation is violated, Fig. 5 shows the backscatter that would be observed by the CALIPSO lidar[7] from an altitude of 700 km. Its half-angle laser divergence of $\rho_l = 0.05$ mrad and half-angle field of view of $\rho_t = 0.065$ mrad yield a footprint at the ground of approximately 90 m. The profile under consideration contains an ice cloud between 4 and 7 km with constant properties in the vertical of $\alpha = 1$ km^{-1} and $a_G = 100$ μm (leading to a $1/e$ scattering angle of $\Theta = 0.0017$ rad). Beneath this lies a 1 km aerosol layer with $\alpha = 0.5$ km^{-1} and $a_G = 0.5$ μm (leading to $\Theta = 0.34$). Both have an extinction-to-backscatter ratio of 20 sr. The thick black line shows $\hat{\beta}$ calculated including the aerosol adjustment described at the end of Section 4, whereby forward scattering from the aerosol layer is considered to be at too large an angle to contribute to the returned signal, except for doubly scattered photons calculated using Eq. (10). The crosses show $\hat{\beta}$ calculated including the effects of aerosol forward scattering.

It can be seen that the backscatter from both the ice cloud and the molecules immediately beneath it are well predicted by the new algorithm (to 3%), and the Eloranta algorithm needs to be taken to at least seventh-order scattering before it converges. In both these regions the backscatter lies close to the wide field-of-view limit.

The performance in and below the aerosol layer is poor when forward scattering from the aerosol layer is included, resulting in a significant underestimate in the molecular return from beneath this layer. This

Table 1. Execution Time of the Various Algorithms Relative to the Time for the New Algorithm to Compute a 25-Point Profile[a,b]

Points in Profile, N	25	50
New algorithm		
Standard formulation	1.0	3.5
With approximate Jacobian	1.9	7.1
Eloranta's algorithm[c]		
Scattering to second order	0.62	2.4
Scattering to third order	5.7	41
Scattering to fourth order	42	550
Scattering to fifth order	250	6000
Scattering to sixth order	1200	54,000

[a]0.16 ms on a 1 GHz Pentium 3.

[b]Values are reported to two significant figures and have been calculated from repeated calls to the core algorithm, thereby excluding any time associated with memory allocation and input–output of data. David Donovan's fast implementation of Eloranta's algorithm was used.

[c]Ref. 9.

is because E_s and E_m in this region are highly non-Gaussian, containing a narrow component due to forward scattering from the ice cloud and a wide component due to forward scattering from the aerosol layer. Most of the multiply scattered returned photons are due to the narrow component, but this is smeared out when the Gaussian approximation is made, resulting in the underestimate shown by the crosses.

However, the aerosol adjustment largely corrects this error, with the thick black line showing a residual underestimate of up to 7% in the layer itself. When the same scene is viewed from below, the backscatter from the aerosol layer is well predicted, but the backscatter of the ice cloud is strongly underestimated if aerosol forward scattering is permitted. Again, this problem is removed by permitting only double scattering from the aerosol layer.

Care should be taken in applying this algorithm to optically thick liquid water clouds observed by lidars with large footprints, such as CALIPSO. Although it is found that the new algorithm agrees reasonably well with that of Eloranta in such clouds (even though the particle size is much smaller than any overlying ice cloud), strictly speaking both algorithms are being applied outside their realm of applicability, as the assumption that the photon mean free path is much longer than the lidar footprint is no longer valid. In these situations, wide-angle scattering, events become important, and the extra path length of multiply scattered photons results in a bleeding effect with a range that is not represented by either algorithm.

6. Speed of the Algorithm

Benchmark computations have been performed to compare the relative speed of the algorithm described in this paper with Eloranta's algorithm for scattering truncated at orders between 2 (double scattering only) and 6. Two profiles were used, one with $N = 25$ gates and the other with $N = 50$ gates, in both cases with every gate containing cloud. The results are shown in Table 1.

Eloranta's algorithm with single and double scattering only (second order) is found to run faster than the new algorithm; the computational time for both is proportional to N^2, but the new algorithm carries the extra overhead of calculating the extra variables to enable the higher-order scattering to be estimated. As expected, when Eloranta's algorithm is truncated at higher orders of scattering the time taken is approximately proportional to $N^m/m!$, where m is the order of scattering. Typically it is found that the new algorithm is as accurate as Eloranta's when truncated to fifth- or sixth-order scattering, and Table 1 shows that for a 50-point profile it is therefore over 3 orders of magnitude faster for the same accuracy.

If the new algorithm is to be implemented in iterative variational retrieval schemes, then the Jacobian needs to be calculated, consisting of a matrix of the partial derivatives of apparent backscatter at each gate with respect to the extinction coefficient and particle size at every gate, i.e., $\partial\hat{\beta}_j/\partial\alpha_i$ and $\partial\hat{\beta}_j/\partial a_{G,i}$. A simple but expensive way to compute this is to run the algorithm $2N$ times, perturbing α or a_G at each gate. A more efficient approach is to work out expressions for the Jacobian by hand and then compute these. It has been found that the Jacobian of the single and double scattering parts of the algorithm [i.e., derivatives of Eqs. (7) and (11)] may be computed with $O(N^2)$ efficiency, but the Jacobian of the triple- and higher-order component would be $O(N^3)$ efficient. Early development of a variational radar–lidar retrieval scheme (to be reported in a future paper) has demonstrated that the approximate Jacobian including only single and double scattering is adequate for rapid convergence because the matrix is diagonally dominant, and the diagonal elements (i.e., $\partial\hat{\beta}_i/\partial\alpha_i$) are still computed accurately. Table 1 shows that the approximate Jacobian may be calculated in around twice the time of the standard algorithm.

7. Conclusions

A new lidar multiple scattering algorithm has been developed that is fast enough to be used in iterative retrieval algorithms applied to large volumes of data such as from spaceborne cloud lidar, while still representing high orders of scattering. This is achieved by a new way of treating the backscatter due to triple- and higher-order scattering. Rather than explicitly modeling all the possible ways that a multiply forward-scattered photon can reach a particular range gate, the photon distribution at a gate is modeled by a handful of variables, including, crucially, the covariance of photon position and direction.

In terms of accuracy the new algorithm compares very well to the much slower Eloranta[9] algorithm truncated at the seventh-order scattering, although problems can arise when layers containing very different particle sizes are present in the same profile and the quasi-small-angle approximation is violated. It has been found that problems associated with aerosols can be dealt with satisfactorily and simply by allowing double scattering only in layers for which $\Theta > 0.1$, although for systems in which the scattering frequently lies near this threshold, a more rigorous approach may be necessary.

The code for the algorithm is freely available for download from the author's Web site (http://www.met.reading.ac.uk/clouds).

I am grateful to Ed Eloranta and David Donovan for the use of their implementations of the Eloranta algorithm, to David Donovan for useful discussions, and to the two anonymous referees for bringing to my attention the equivalent-medium theorem that helped to simplify the description of the algorithm.

References

1. C. M. R. Platt and A. C. Dilley, "Remote sounding of high clouds—4. Observed temperature variations in cirrus optical properties," J. Atmos. Sci. **38,** 1069–1082 (1981).
2. M. Chiriaco, H. Chepfer, V. Noel, A. Delaval, M. Haeffelin, P. Dubuisson, and P. Yang, "Improving retrievals of cirrus cloud particle size coupling lidar and three-channel radiometric techniques," Mon. Weath. Rev. **132,** 1684–1700 (2004).
3. D. P. Donovan, A. C. A. P. van Lammeren, H. W. J. Russchenberg, A. Apituley, R. J. Hogan, P. N. Francis, J. Testud, J. Pelon, M. Quante, and J. W. F. Goddard, "Cloud effective particle size and water content profile retrievals using combined lidar and radar observations—2. Comparison with IR radiometer and *in situ* measurements of ice clouds," J. Geophys. Res. **106**(D21), 27449–27464 (2001).
4. C. Tinel, J. Testud, R. J. Hogan, A. Protat, J. Delanoe, and D. Bouniol, "The retrieval of ice cloud properties from cloud radar and lidar synergy," J. Appl. Meteorol. **44,** 860–875 (2005).
5. R. J. Hogan, D. P. Donovan, C. Tinel, M. A. Brooks, A. J. Illingworth, and J. P. V. Poiares Baptista, "Independent evaluation of the ability of spaceborne radar and lidar to retrieve the microphysical and radiative properties of ice clouds," J. Atmos. Ocean. Technol. **23,** 211–227 (2006).
6. C. D. Rodgers, *Inverse Methods for Atmospheric Sounding: Theory and Practice* (World Scientific, 2000).
7. D. M. Winker, J. Pelon, and M. P. McCormick, "The CALIPSO mission: spaceborne lidar for observation of aerosols and clouds," in Proc. SPIE **4893,** 1–11 (2003).
8. G. L. Stephens, D. G. Vane, R. J. Boain, G. G. Mace, K. Sassen, Z. Wang, A. J. Illingworth, E. J. O'Connor, W. B. Rossow, S. L. Durden, S. D. Miller, R. T. Austin, A. Benedetti, C. Mitrescu, and the CloudSat Science Team, "The CloudSat mission and the A-Train," Bull. Am. Meteorol. Soc. **83,** 1771–1790 (2002).
9. E. W. Eloranta, "A practical model for the calculation of multiply scattered lidar returns," Appl. Opt. **37,** 2464–2472 (1998).
10. L. R. Bissonnette, "Lidar and multiple scattering," in *Lidar Range-Resolved Optical Remote Sensing of the Atmosphere,* C. Weitkamp, ed. (Springer, 2005), pp. 43–103.
11. L. R. Bissonnette, "Multiple-scattering lidar equation," Appl. Opt. **35,** 6449–6465 (1996).
12. I. L. Katsev, E. P. Zege, A. S. Prikhach, and I. N. Polonsky, "Efficient technique to determine backscattered light power for various atmospheric and oceanic sounding and imaging systems," J. Opt. Soc. Am. A **14,** 1338–1346 (1997).
13. H. C. van de Hulst, *Light Scattering by Small Particles* (Dover, 1981).